Event-Based Beam Tracking with Dynamic Beamwidth Adaptation in Terahertz (THz) Communications

Yasemin Karaçora*, *Graduate Student Member, IEEE*, Christina Chaccour†, *Member, IEEE*, Aydin Sezgin*, *Senior Member, IEEE*, and Walid Saad†, *Fellow, IEEE*
* Institute of Digital Communication Systems, Ruhr University Bochum, Germany,
†Bradley Department of Electrical and Computer Engineering, Virginia Tech, Arlington, USA
Emails: {yasemin.karacora, aydin.sezgin}@rub.de, christinac@ieee.org, walids@vt.edu

***Abstract*—Terahertz (THz) communication will be a key enabler for next-generation wireless systems. While THz frequency bands provide abundant bandwidth and extremely high data rates, their effective operation is inhibited by short communication ranges and narrow beams, thus, leading to major challenges pertaining to user mobility, beam alignment, and handover. In particular, there is a strong need for novel beam tracking methods that consider the tradeoff between enhancing the received signal strength via increasing beam directivity, and increasing the coverage probability by widening the beam. In this paper, a multi-objective optimization problem is formulated with the goal of jointly maximizing the expected rate and minimizing the outage probability subject to transmit power and overhead constraints. Subsequently, a novel parameterized beamformer with dynamic beamwidth adaptation is proposed. In addition to the precoder, an event-based beam tracking approach is introduced that efficiently prevents outages caused by beam misalignment and dynamic blockage while maintaining a low pilot overhead. Simulation results show that the proposed beamforming scheme improves average rate performance and reduces the amount of outages caused by the brittle THz misalignment process and the particularly severe path loss in the THz band. Moreover, the proposed event-triggered THz channel estimation approach enables connectivity with minimal overhead and reliable communication at THz bands.**

***Index Terms*—Terahertz (THz), beamforming, beam tracking, beamwidth, reliability, overhead, 6G systems**

I. Introduction

A fundamental characteristic of next-generation wireless 6G networks is the migration towards higher frequency bands, namely the terahertz (THz) band (0.1–10 THz)[1]. Wireless communication links at the THz frequency bands benefit from an abundant bandwidth which enables extremely high data rates (in the order of Tbps) that are essential for future 6G services like extended reality (XR) [1] or digital twins [2]. However, unleashing the true potential of THz frequency bands necessitates overcoming key THz challenges, stemming from the channel's uncertainty. Particularly, two major factors that restrain the communication at THz bands are the high path loss and the molecular absorption effect [3], [4]. More specifically, such factors can potentially increase the channel attenuation by more than 20 dB when migrating from a carrier frequency of 30 GHz up to 300 GHz. To compensate the effect of these phenomena, a very narrow beam (so-called pencil beam) is needed to focus the power towards the receiver [5]. Nonetheless, the communication reliability is at risk when using a narrow beam due to potential blockages and beam misalignment. Indeed, even slight changes in target direction (within a few degrees or less) can result in communication outages, especially in dynamic use cases. While this phenomenon can affect mmWave communication, it becomes substantially more pronounced in (sub-)THz systems. Due to the extremely high path loss, as well as the molecular absorption caused by water vapor, the THz band is more suitable for indoor environments with shorter ranges ($\leq$ 20 m), lower levels of humidity, and thus stronger communication links [3]. While indoor environments may be more favorable, the reliability of THz links remains affected by beam misalignments resulting from changes in the micro-mobility of users [6], [7]. Henceforth, investigating the tradeoff between the pathloss compensation and the mitigation of beam misalignment is substantially crucial for the deployment of THz bands [8]. Indeed, the optimal tradeoff adjustment could ultimately lead to the delivery of *reliable and robust THz links in dynamic environments*, a fundamental necessity for 6G services like XR [1].

In order to maintain system reliability and prevent communication outages, beam tracking algorithms must provide very precise and timely channel state information (CSI). However, frequent pilot transmissions could induce a significant overhead that restricts the transfer of large amounts of data with low latencies [6]. This challenge is further exacerbated by the large antenna arrays needed at THz frequencies to form narrow beams. Thus, developing a resilient beamforming scheme that can adapt to uncertainties in CSI is crucial to guarantee reliable low-overhead THz communication links. Consequently, the

Manuscript received August 19, 2022; revised March 4, 2023 and May 27, 2023; accepted July 5, 2023.

This research was supported, in part, by the Federal Ministry of Education and Research (BMBF) of the Federal Republic of Germany under Grant 16KISK037 (6GEM), by the Ministry of Economic Affairs, Industry, Climate Action and Energy of the State of North Rhine-Westphalia, Germany under grant 005-2108-0028 (5G-Furios), and by the U.S. National Science Foundation under Grants CNS-1836802 and CNS-2225511.

[1]The frequency range 100 – 300 GHz is typically referred to as the sub-THz band, while the unique properties of the THz band are observed above 275 GHz. However, in this work the term THz is used to refer to the overall range 0.1 – 10 THz.

tradeoff between providing sufficient communication range with a highly focused beam versus increasing the probability of coverage by generating a wider beam is a key challenge in THz beamforming [8]. Furthermore, since THz channels are highly susceptible to (micro-)mobility as well as the deployment of large antenna arrays, periodic beamforming as adopted in 5G New Radio may be incapable of balancing the tradeoff between mitigating the overhead-induced rate loss and avoiding beam misalignment. Thus, a paradigm shift towards efficient, non-periodic beam realignment schemes is an essential building block for THz communication. Essentially, pilot-based channel measurements must be performed in an event-driven manner so as to handle the highly varying THz channel, while consistently maintaining low latencies and overhead.

A. Prior Art

The challenge of guaranteeing beam alignment of highly directive beams in mmWave and THz systems with user mobility has been addressed in [6]–[20]. For instance, in [6]–[8], the impact of beam misalignment on THz link performance is investigated for different mobility scenarios. These works demonstrate the susceptibility of THz systems to small-scale user mobility and, hence, the need for reliable schemes with regard to time-varying channels. Beam alignment and tracking approaches have been proposed to enhance data rate and reliability in mmWave and THz bands in [9] and references therein. In [10], [11] the problem of beam discovery in THz systems with directional antennas has been studied from a networking perspective. The authors in [10] propose a neighbor discovery protocol based on the antenna radiation pattern and side-lobe information. The work in [11] exploits a single leaky wave antenna to find the dominant propagation paths in the network. The protocols were experimentally validated at 60 GHz [10] and up to 350 GHz [11]. From a physical layer perspective, the highly varying THz channel makes it particularly challenging to maintain an uninterrupted connection beyond the initial access, especially with mobility. Since THz communication relies on pencil beams to overcome the path loss, beam tracking at THz bands yields a large overhead. Methods to reduce the beam training time and the number of pilot signals were developed in [12] based on a hierarchical codebook and in [13], where frequency-dependent precoding is used. While [10]–[13] reduce the overhead of the beam search itself, the total overhead is also primarily determined by how often channel estimation and beam realignment have to be performed. This motivates the need for an optimal choice of the beam realignment intervals in THz communication in order to avoid overhead-induced rate loss on the one hand and outages caused by beam misalignment as a consequence of micro-mobility on the other hand, which has been demonstrated in [6]. The authors in [14] analyze outage probability and spectral efficiency for periodic and on-demand beam searching methods in THz systems with micro-mobility. In [15] beam training is initiated if the received signal power drops below a threshold, whereas in [16] and [17], the training frequency is determined based on the beamwidth and an estimate of the angular velocity.

Although the solutions of [12]–[17] could reduce the training overhead, the time steps during which beam training is initiated are either periodic, follow an on-demand approach, which reacts to outages but is not preventive, or are based on a heuristic threshold. In contrast, a proactive and reactive event-based strategy that *optimizes* the beam realignment intervals based on the channel state and mobility as we propose is crucial to enable reliable communication in the face of the extremely susceptible THz channel while avoiding delays and rate loss induced by pilot overhead. Meanwhile, despite adopting different beamwidths during grid-based search, the works in [12], [13], [15], [16] do not adapt the transmission beamwidth to the estimation uncertainty in the time intervals between training.

While beam tracking approaches can certainly improve channel estimation accuracy and thereby reduce the occurrence of antenna misalignment with a moderate pilot overhead, the beamforming concept itself needs to be robust in the face of remaining channel uncertainties of the highly fluctuating THz channel. Such a robust beamforming design not only enhances communication reliability, but also requires less frequent channel measurements, thus reducing the overhead even further. In [18], the beamwidth tradeoff has been studied for mmWave systems, yet instead of optimizing the beamwidth, the beam is widened step by step until a minimum average signal strength is obtained at the receiver. The relationship between optimal beamwidth and channel uncertainty in a mmWave system is studied in [19] and [20]. The authors in [19] propose a chirp-sequence-based precoder to adapt the beamwidth to the current uncertainty of the user's direction to maximize the ergodic data rate. They show that a wider beam can increase the expected rate if the estimation of the angle of departure (AoD) becomes inaccurate and the signal-to-noise-ratio (SNR) is sufficiently high. While they only consider long-term average rate performance, transmission failures caused by beam misalignment can severely impede continuous data transfer. Hence, communication reliability should be captured by the performance metrics, e.g., by considering outage probability along with the rate. The idea of increasing robustness by dynamically adapting the beamwidth to the current CSI uncertainty has been applied to a mmWave beam tracking scenario in [20]. Therein, the beamwidth is adjusted by activating only part of the antenna array, while the number of active antennas follows a heuristic approach based on the angular deviation. However, the work in [20] is not suitable for THz systems, as it does not include the adaptation of the beamwidth to the channel gain, which is highly affected by user mobility as well as the molecular absorption effect. In a nutshell, the existing mmWave approaches [18]–[20] are not effective in simultaneously providing high data rates and high reliability for THz systems. In essence, such systems do not consider the path loss compensation - beam alignment tradeoff while optimizing their network. Furthermore, the existing works that adopt low overhead tracking propose heuristic approaches and fail to optimize the CSI estimation time intervals. Clearly, such schemes cannot guarantee overhead limitations while simultaneously adjusting to changes in the channel, mobility pattern, and transmissions scheme.

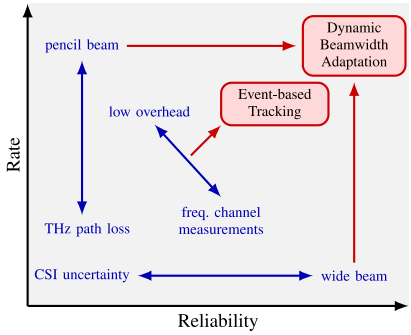

(a) Rate-reliability tradeoff illustration

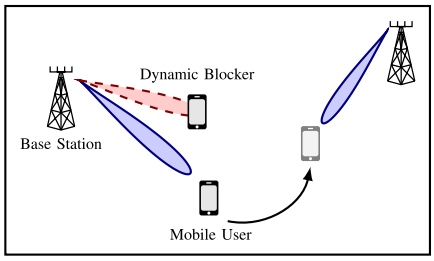

(b) Indoor THz communication network

Fig. 1: (a) Impact of beamwidth and overhead on the rate-reliability tradeoff in THz systems. Our proposed approach comprising a reliable beamforming scheme and an optimized tracking via event times enable the counteraction of path loss and beam misalignment, (b) Downlink transmission to a mobile UE. Other users are potential blockers to the considered communication link, while other BSs can take over serving the user, e.g., if a blockage occurs.

B. Contributions

The main contribution of this paper is the design of a new, low-overhead beamforming and tracking scheme that enhances communication reliability while addressing the peculiar challenges of the THz band. Given that the severe path loss in THz bands requires the use of narrow beams and a high-resolution codebook, THz beam search entails a considerable amount of overhead [9]. Thus, we propose a beamforming design that accounts for the highly varying nature of the THz channel by addressing the tradeoff between THz path loss compensation and beam alignment, and provides robust and reliable communication with minimal overhead (see Fig. 1(a)). In this work, we consider the downlink of an indoor wireless THz network with a dense base station (BS) deployment and multiple mobile user equipments (UEs) that are subject to dynamic channel blockage (Fig. 1(b)):

- *Multi-objective optimization:* We aim at optimizing the beamformer and the time steps at which pilot-based channel estimation is performed, in order to provide reliable communication at high data rates, while maintaining a low overhead (see Fig. 1(a)). We formulate an optimization problem that aims at jointly maximizing the expected data rate and minimizing the outage probability, subject to constraints on the transmit power and the long-term average overhead. Applying linear scalarization to the multi-objective problem enables balancing high rate and reliability requirements according to the application. The problem is then split into two subproblems to solve for the beamformer and the pilot event times separately.
- *Path loss vs. misalignment tradeoff:* We propose a novel beamforming scheme that is reliable in front of CSI uncertainties. In order to reduce the computational complexity of our precoding, we propose a parameterized beamformer with adjustable beamwidth. Combining this with a small-angle approximation allows us to solve the optimization problem in advance and generate a lookup table for the optimal beam parameters, which dynamically adjust the beamwidth depending on the current channel uncertainty and path loss.
- *Event-trigger for overhead reduction:* To ensure reliable communication by further minimizing beam misalignments without violating the average overhead constraint, we adopt the concept of event-triggered communication, that enables more efficient scheduling of pilots. Instead of periodically transmitting pilot signals for channel estimation, the interval between consecutive channel measurements is dynamically adapted to the current system state. Here, we adopt a Lyapunov optimization framework to determine the time steps, at which the BS receives updates on the UE's current direction. This enables a flexible system capable of not only reacting to outage events when needed but preventing outages by ensuring sufficiently accurate CSI while still complying with a given average overhead constraint.
- *Beamforming scheme analysis:* We analyze the proposed beamforming scheme by numerically calculating the Pareto boundary of the two objectives, namely expected data rate and outage probability, for a general beamformer and compare it to the achievable Pareto region of our proposed parameterization. We further gain insights regarding the optimal beamwidths for different BS-UE distances and uncertainty of the UE's position as well as the impact of the molecular absorption effect in the THz band. Here, we observe that the optimal beamforming strategy differs significantly for the two considered objectives. Moreover, our approach is shown to outperform state-of-the-art variable beamwidth schemes.
- *Analysis of event-based tracking procedure:* The performance of our event-based tracking scheme combined with the proposed beamforming approach is evaluated and compared to a non-robust periodic scheme. Our approach is shown to significantly reduce the amount of outage events while requiring much less pilot overhead.

The rest of this paper is organized as follows. In Section II the channel model and UE's mobility model are introduced. Then, in Section III, the proposed robust beamforming scheme is presented. Section IV describes the event-based channel estimation and tracking approach. Section V presents the simulation results and, finally, conclusions are drawn in Section VI.

Notation: Vectors and matrices are denoted by boldface lowercase and uppercase letters, respectively. The operators $\mathbb{E}[\cdot]$, $|\cdot|$ and $\lfloor\cdot\rfloor$ represent the expectation, the absolute value and the floor function, respectively. $\boldsymbol{X}^T$ and $\boldsymbol{X}^H$ are the transpose and the hermitian, while $[\boldsymbol{X}]_{m,n}$ denotes the element in the m-th row and n-th column of $\boldsymbol{X}$.

II. System Model

Consider a multiple-input-multiple-output (MIMO) THz communication system, where multiple BSs, which are densely deployed in an indoor area, are transmitting data to multiple mobile UEs. Each BS (UE) is equipped with a uniform linear array (ULA) consisting of N_{t} (N_{r}) antennas. We focus on the downlink of a single mobile UE i and its associated serving BS j (see Fig. 1(b)). From this perspective, other users take the role of potential blockers. Hence, communication is jeopardized for three main reasons, namely beam misalignment caused by the UE's mobility, dynamic blockage induced by other users, and the user moving out of the communication range of the BS. To cope with these impairments, the BS-UE channel is estimated based on pilot measurements on a regular basis. Additionally, the mobile user can be handed over to another BS if coverage is disrupted.

A. Channel Model

We adopt the Saleh-Valenzuela channel model, that is widely used for THz communications (e.g., see [5], [12], [15]) and generally consists of one line-of-sight (LOS) path and a few reflection paths as follows:

$$\begin{aligned}\boldsymbol{H}_k =&\gamma_k^{(0)}\eta(d_k^{(0)})\boldsymbol{a}_{\mathrm{r}}(\varphi_{\mathrm{r},k}^{(0)})\boldsymbol{a}_{\mathrm{t}}^H(\varphi_{\mathrm{t},k}^{(0)})\\ &+\sum_{l=1}^{L}\gamma_k^{(l)}\eta(d_k^{(l)})\boldsymbol{a}_{\mathrm{r}}(\varphi_{\mathrm{r},k}^{(l)})\boldsymbol{a}_{\mathrm{t}}^H(\varphi_{\mathrm{t},k}^{(l)}),\end{aligned} \tag{1}$$

where k is the time index and L is the number of reflection paths. While $\eta(\cdot)$ is the path gain, $d_k^{(0)}$ and $d_k^{(l)}$ represent the length of the LOS path and the l-th reflection path, respectively. The AoD and angle of arrival (AoA) of the l-th path are denoted by $\varphi_{\mathrm{t}}^{(l)}$ and $\varphi_{\mathrm{r}}^{(l)}$, respectively. The transmit and receive array response vectors are $\boldsymbol{a}_{\mathrm{t}}(\cdot)$ and $\boldsymbol{a}_{\mathrm{r}}(\cdot)$. We capture the effect of blockage by defining a random binary variable $\gamma_k^{(l)}$, that is equal to one if the l-th link exists at time step k and equal to zero if it is blocked. Without loss of generality, we assume the antenna spacing to be half of a wavelength. Hence, the array response vectors are defined as:

$$\boldsymbol{a}(\varphi)=\frac{1}{\sqrt{N}}\left[1,\ e^{j\pi\sin(\varphi)},\dots,e^{j\pi(N-1)\sin(\varphi)}\right]^T. \tag{2}$$

At THz frequencies, in addition to the free space propagation loss, the path loss is highly affected by molecular absorption. Hence, the total channel gain is given by [21]:

$$\eta(d_k)=\frac{c}{4\pi f d_k}e^{-\frac{1}{2}K(f)d_k}, \tag{3}$$

where f is the carrier frequency, c is the speed of light, and $K(f)$ represents the overall absorption coefficient of the medium. We obtain $K(f)$ for the frequency range of 100 – 450 GHz based on the model presented in [22]. At time step k, the BS transmits the symbol s_k with $\mathbb{E}[|s_k|^2]=1$. The received signal will be given by:

$$y_k=\boldsymbol{w}_k^H\boldsymbol{H}_k\boldsymbol{f}_k s_k+n_k, \tag{4}$$

where $\boldsymbol{f}_k$ and $\boldsymbol{w}_k$ are the precoder and combiner, respectively, and $n_k\sim\mathcal{CN}(0,\sigma_{\mathrm{n}}^2)$ is additive white Gaussian noise (AWGN). Here, the noise power $\sigma_{\mathrm{n}}^2=N_0+P_{\max}\left(\frac{c}{4\pi f d_k}\right)^2(1-e^{-K(f)d_k})$ is the sum of the thermal noise power $N_0=\frac{W\lambda^2}{4\pi}k_{\mathrm{B}}T_0$ with the Boltzmann constant k_{B} and the temperature T_0 in Kelvin, and molecular absorption noise caused by molecular re-radiation [21], [23]. The achievable data rate with bandwidth W can be written as:[2]

$$R_k=W\log_2\left(1+\frac{1}{\sigma_{\mathrm{n}}^2}\boldsymbol{w}_k^H\boldsymbol{H}_k\boldsymbol{f}_k\boldsymbol{f}_k^H\boldsymbol{H}_k^H\boldsymbol{w}_k\right). \tag{5}$$

Due to the LOS dominance in the THz channel, the precoder and combiner would ideally be designed to align the beam in LOS direction, or, in case of LOS blockage, in the direction of the strongest reflection path. Given the narrow beams utilized in THz frequency bands, the power received through reflections and scattering from different angles other than the main lobe direction is negligible [25]. As such, we also neglect interference caused by other devices. Hence, since only the strongest path is exploited for transmission, we approximate the channel by

$$\boldsymbol{H}_k\approx\gamma_k\eta(d_k)\boldsymbol{a}_{\mathrm{r}}(\varphi_{\mathrm{r},k})\boldsymbol{a}_{\mathrm{t}}^H(\varphi_{\mathrm{t},k}), \tag{6}$$

where d_k, $\varphi_{\mathrm{t},k}$ and $\varphi_{\mathrm{r},k}$ are the distance, the AoD and AoA of the LOS link or of the strongest available NLOS path (in case of a blocked LOS path), respectively. In fact, from the BS's perspective, the NLOS case can be handled in the same way as a LOS path towards a virtual UE that is located at the reflection of the UE with respect to the reflective surface [26], where the distance is equal to the total length of the reflection path. We define γ_k as the blockage variable of the channel at time slot k. This is because the precoder and combiner are fixed for the duration of one time slot, thus, blockage of the LOS path results in a communication outage even if a reflection path is available. The beamformer needs to be aligned with the NLOS path first to reestablish the connection in the next time slot. We introduce the blockage model next.

B. Blockage model

Given that the THz frequency band suffers from high penetration losses, the THz channel is highly susceptible to blockages, which, as a result, lead to a severe decline of the received signal power and thus jeopardize the system reliability. We distinguish different types of blockages based on their source (self-blockage vs. blockage caused by other objects) and their temporal occurrence (static vs. dynamic). We assume that static blockages are easily avoidable by appropriate positioning of the BSs and successful initial access. Hence, we consider the more relevant dynamic blockages and restrict our model to those caused by other mobile users in a dense network, whereas self-blockage is neglected for the scope of this work. We model dynamic blockage as an M/M/∞ queuing system [21], [27]. Based on the assumption that the blocked and unblocked time intervals are independent of each other, blockage can be modeled as an alternating renewal process. More specifically, the occurrence of dynamic blockages is modeled as a Poisson process with arrival rate

[2]Note that in this work, we neglect the wideband beam squint effect as it can be compensated very well when a delay-phase precoding architecture is used [24].

κ_{B} blockers/sec and an exponentially distributed blockage duration with parameter μ_{B}.[3] That is, the binary LOS blockage variable γ_k follows an exponential on-off process with κ_{B} and μ_{B} as the blocking and unblocking rate, respectively. The corresponding blocking and unblocking probabilities are

$$\begin{aligned} P(\gamma_k = 0|\gamma_{k-1} = 1) &= 1 - e^{-\kappa_{\mathrm{B}}(d_k)T_{\mathrm{s}}}, \text{ and} \\ P(\gamma_k = 1|\gamma_{k-1} = 0) &= 1 - e^{-\mu_{\mathrm{B}}T_{\mathrm{s}}}, \end{aligned} \tag{7}$$

where T_{s} is the length of a single time slot. While the unblocking rate μ_{B} is assumed to be a constant parameter known by the BS, the blockage arrival rate depends on the distance between BS and UE and is obtained according to [27, Lemma 1] as:

$$\kappa_{\mathrm{B}}(d_k) = \frac{2}{\pi}\lambda_{\mathrm{B}} v_{\mathrm{B}} \frac{h_{\mathrm{B}} - h_{\mathrm{UE}}}{h_{\mathrm{BS}} - h_{\mathrm{UE}}} d_k, \tag{8}$$

where λ_{B} denotes the density of dynamic blockers per m^2 and v_{B} is the blockers velocity. Here, h_{B}, h_{UE}, and h_{BS} represent, respectively, the height of the blocker, the considered UE, and the BS. Note that the blockage of a NLOS path can be modeled in the same way as for a LOS path based on the equivalent virtual user LOS representation [26]. The user mobility is modeled next.

C. Mobility Model

We model the UE's mobility as a random walk (RW) [6], [29], where the steps in x- and y-direction are independently and identically distributed (i.i.d.) as $\mathcal{N}(0, \sigma_{\mathrm{m}}^2)$. For simplicity, we consider the trajectory of the UE in the horizontal x-y-plane only, while omitting the height. Assuming that users in an indoor scenario oftentimes do not walk towards a specific destination and frequently change directions, the RW model arises as a useful and tractable mobility model for our considered scenario, although our scheme can generally work with other mobility models as well. Moreover, beyond the need to know the statistical model parameter, i.e., the average step size, which can be learned prior to transmission from historical data collected by the BS [30], specific knowledge of the UE's movement behavior (such as instantaneous velocity and moving direction) is not required at the BS when considering RW models.

Due to the impact of user mobility on the channel, the BS relies on regular channel estimations at the cost of pilot overhead to adjust the beam accordingly. In order to capture the intermittent CSI updates, we define a binary variable q_k, which is equal to one whenever the BS obtains a new channel estimate and is equal to zero in between those updates. Given the geometric channel model, the BS is assumed to obtain perfect knowledge of the current AoD and distance of the UE when $q_k = 1$. Let $\boldsymbol{p}_k = [d_k \cos(\varphi_{\mathrm{t},k}),\ d_k \sin(\varphi_{\mathrm{t},k})]^T$ be the position vector of the UE at time step k, where d_k and $\varphi_{\mathrm{t},k}$ denote the current UE's distance to the BS and the AoD, respectively. Then, the position estimate at the BS will be given by:

$$\hat{\boldsymbol{p}}_k = \begin{cases} \boldsymbol{p}_k, & \text{if } q_k = 1, \\ \hat{\boldsymbol{p}}_{k-1}, & \text{if } q_k = 0. \end{cases} \tag{9}$$

Given that the user mobility is modeled as a RW with Gaussian step size, the estimation error $\boldsymbol{e}_k = \boldsymbol{p}_k - \hat{\boldsymbol{p}}_k$ is the sum of M_k i.i.d. Gaussian steps, where M_k is the number of time slots since the BS received the most recent update of the user's position. Hence, $\boldsymbol{e}_k$ also follows a Gaussian distribution with $\mathcal{N}(\boldsymbol{0}, \sigma_{\mathrm{p},k}^2 \boldsymbol{I})$, and the variance is given as $\sigma_{\mathrm{p},k}^2 = M_k \sigma_{\mathrm{m}}^2$ [31].

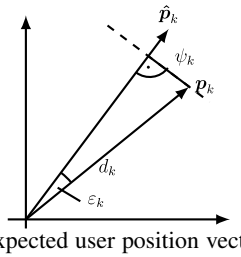

Fig. 2: Geometry of expected user position vector $\hat{\boldsymbol{p}}_k$, actual position $\boldsymbol{p}_k$ and AoD estimation error ε_k, assuming that the BS is located at the origin.

Let $\varepsilon_k = \varphi_{\mathrm{t},k} - \hat{\varphi}_{\mathrm{t},k}$ be the AoD estimation error. As the distribution of ε_k is quite complex (see [32] for the exact distribution), we show that it can be approximated by a normal distribution for small ε_k in what follows. Note that the assumption of small AoD errors is reasonable, since even small deviations of the AoD are critical given the narrow beams in THz communication. From Figure 2, we obtain $\frac{\psi_k}{d_k} = \sin(\varepsilon_k) \approx \varepsilon_k$, where ψ_k is the component of the location error $\boldsymbol{e}_k$, which is orthogonal to $\hat{\boldsymbol{p}}_k$ and $d_k \gg \psi_k$. Since the distribution of the position estimation error is circular symmetric, we know that $\psi_k \sim \mathcal{N}(0, \sigma_{\mathrm{p},k}^2)$. By further approximating d_k by $\hat{d}_k$, for small ε_k, we can assume $\varepsilon_k \sim \mathcal{N}(0, \sigma_{\mathrm{p},k}^2/\hat{d}_k^2)$. Note that the AoD estimation error following a normal distribution is a common assumption in other works on beam tracking as well, such as in [20], [33]–[35]. Hence, with $\sigma_{\varepsilon,k}^2 = \sigma_{\mathrm{p},k}^2/\hat{d}_k^2$, we define the probability density function (PDF) of ε_k as:

$$g_k(\varepsilon_k) = \frac{1}{\sqrt{2\pi\sigma_{\varepsilon,k}^2}} \exp\left(-\frac{\varepsilon_k^2}{2\sigma_{\varepsilon,k}^2}\right). \tag{10}$$

Note that, again, the distribution of the AoD estimation error can be directly transferred to reflection paths as well by considering an equivalent LOS path towards a virtual UE instead.

D. Tracking and Problem Statement

Our goal is to design a beamforming scheme that enables reliable communication despite the uncertainty of the user's location while maintaining a low channel estimation overhead. The problem is formulated from the perspective of a single UE and its associated BS, while other users are considered as potential dynamic blockers and other BSs can take over serving the UE if it moves out of range or in case of link blockage. The BS obtains the current CSI and UE's location through pilot measurements, which are initiated in a non-periodic event-triggered manner to comply with a maximum

[3]Assuming that the blockers' distribution is a Poisson point process, the blockage process would ideally be modeled as an M/G/∞ queue as in [28], i.e., the blockage duration follows a general distribution. However, for tractability, we adopt the assumption from [27], that the blockage duration is exponentially distributed, which relaxes the model to an M/M/∞ queue.

average overhead constraint.[4] In between CSI updates, the BS transmits data to the UE while adjusting the beamformer in every time slot based on the available statistical CSI. We define *communication outages* as the event of the achievable data rate R_k falling below a given target rate $R_{\min}$. Note that outages caused by insufficient signal strength at the receiver can occur in multiple ways: First, CSI at the BS is not always accurate, since user mobility in a non-static environment leads to a fast varying channel. As a result, beams are not perfectly aligned, which can cause communication outages. This effect is aggravated due to the very narrow beams commonly used to overcome the severe path loss in THz channels. Second, the high penetration loss at THz bands leads to blockages, particularly caused by other users in a mobile environment. Due to the highly focused beams, a blockage of the current transmission path first leads to a communication outage even in a multipath channel. Furthermore, if the LOS link is blocked and no sufficiently strong reflection path is available, the target rate cannot be supported by the channel. Beyond that, an outage can occur as a result of an excessive path loss when the UE moves out of the THz communication range of the BS. While the BS can react to outages with a new channel measurement or a handover, we aim at designing a robust beamforming scheme, that provides high data rates despite inaccurate CSI and severe THz path loss and reduces the probability of outages caused by beam misalignment.

A suitable performance metric to consider in communication scenarios with imperfect CSI at the transmitter is the expected data rate. Maximizing $\mathbb{E}[R]$ can provide a relatively high average system throughput despite channel uncertainties. However, the expected rate metric alone can conceal interruptions in communication (outages or temporary rate decline). Indeed, many THz communication use-cases, such as XR applications, not only require high data rates (e.g., to deliver visual content), but also depend on a continuous and timely data transfer to provide a seamless user experience. A useful metric to capture these instantaneous QoS violations is the probability of outage. A communication scheme designed to reduce the outage probability ensures consistent data transfer at the expense of total throughput. Due to its threshold-based definition, outage probability is also vulnerable to channel uncertainties. Given the highly susceptible THz channel and the user mobility in our considered communication setup, outages are likely to occur. In order to provide high data rates despite channel uncertainties, yet avoid outages caused by beam misalignment, we formulate a multi-objective optimization problem [36], [37]. In addition to the beamforming scheme, we also aim at optimizing the time steps, at which a new pilot measurement is performed. This enhances efficiency of the tracking procedure by enabling timely CSI updates to prevent outages, yet maintaining a low overhead. Hence, our goal is to optimize the beamformer and the pilot measurement times with regard to the expected data rate and the outage probability, subject to constraints on the transmit power and the long-term average pilot overhead. Mathematically, we have the following multi-objective optimization problem:

$$\max_{\boldsymbol{f}_k,\, q_k} \quad \left(\mathbb{E}\left[R_k|\boldsymbol{f}_k, q_k\right],\ -\Pr(R_k < R_{\min}|\boldsymbol{f}_k, q_k)\right) \tag{11}$$

$$\text{s.t.} \quad \boldsymbol{f}_k^H \boldsymbol{f}_k \leq P_{\max}, \tag{12}$$

$$\lim_{K\to\infty} \frac{1}{K} \sum_{k=1}^{K} q_k \leq r_{\mathrm{q}}, \tag{13}$$

where $P_{\max}$ denotes the maximum transmit power and r_{q} represents the allowable average channel estimation overhead. Note that in the evaluation, we demonstrate that each of the two objectives considered by itself leads to substantially different beamforming strategies. The problem is converted into a single-objective optimization problem through scalarization [36] as follows:

$$\begin{aligned} \max_{\boldsymbol{f}_k,\, q_k} \quad & g_\alpha(\boldsymbol{f}_k, q_k) \\ \text{s.t.} \quad & (12),\ (13), \end{aligned} \tag{14}$$

in which the objective function is chosen to be a weighted sum of the two objectives, given by:

$$g_\alpha(\boldsymbol{f}_k, q_k) = \alpha\, \frac{\mathbb{E}\left[R_k|\boldsymbol{f}_k, q_k\right]}{R_{\max}} - (1-\alpha)\Pr(R_k < R_{\min}|\boldsymbol{f}_k, q_k), \tag{15}$$

where $\alpha \in [0, 1]$ is a design parameter, which balances the two objectives. In order to make the two metrics comparable, in (15), the expected data rate is normalized by $R_{\max}$, which is an approximation of the maximum expected rate [37]. This makes both objectives in the weighted sum dimensionless values between 0 and 1. $R_{\max}$ is chosen to be the achievable rate with perfect CSI available at the transmitter. Hence, it is obtained as follows:

$$R_{\max} = W \log_2 \left(1 + \frac{P_{\max}\eta^2(\hat{d}_k)}{\sigma_{\mathrm{n}}^2}\right). \tag{16}$$

In the following two sections, the optimization problem in (14) is split into two subproblems, optimizing the beamforming vector $\boldsymbol{f}_k$ first, and then deriving a dynamic condition that triggers the pilot measurements by optimizing the channel estimation variable q_k.

III. Reliable Variable-Beamwidth Precoding

Given that the BS's location is fixed, we assume that the UE is aware of its own position relative to the BS, i.e., the current AoA $\varphi_{\mathrm{r},k}$ is available at the UE. Thus, the UE will apply maximum ratio combining to the received signal, so that:

$$\boldsymbol{w}_k = \frac{\boldsymbol{a}_{\mathrm{r},k}(\varphi_{\mathrm{r},k})}{||\boldsymbol{a}_{\mathrm{r},k}(\varphi_{\mathrm{r},k})||}. \tag{17}$$

Note that when $q_k = 1$, i.e., a new channel measurement has been performed at the beginning of time step k and, hence, the BS is assumed to have perfect CSI, a maximum ratio transmitting strategy would be optimal. Therefore, we first solve the precoding optimization problem for the case of imperfect CSI, i.e., for $q_k = 0$ with the overhead constraint (13) becoming irrelevant for this subproblem. Similarly, since we assume that blockage of the current transmission path (i.e., $\gamma_k = 0$) always causes an outage, blockages can be

[4]Note that our focus lies on the beam tracking procedure and not on initial access, which is why we consider the overhead arising in the user (data) plane rather than control plane.

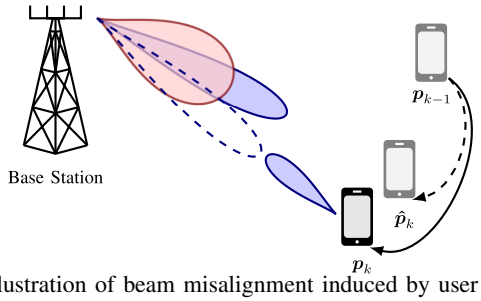

Fig. 3: Illustration of beam misalignment induced by user mobility.

ignored when optimizing the beamformer. The optimization of q_k including blockages is covered in Section IV-A. Thus, with these assumptions and the combiner in (17), the subproblem for beamforming optimization can be written as:

$$\begin{aligned} \max_{\boldsymbol{f}_k} \quad & g_\alpha(\boldsymbol{f}_k, q_k = 0) \\ \text{s.t.} \quad & (12), \end{aligned} \tag{18}$$

while the rate expression in (5) reduces to

$$R_k = W \log_2 \left(1 + \frac{\eta^2(d_k)}{\sigma_{\mathrm{n}}^2} \left|\boldsymbol{a}_{\mathrm{t}}^H(\varphi_{\mathrm{t},k}) \boldsymbol{f}_k\right|^2\right). \tag{19}$$

Note that (18) is a challenging problem, since it is non-convex and the expectation operator in the objective function cannot be solved in closed form. Additionally, the optimal precoder highly depends on the communication distance and the AoD distribution, which requires constant recalculation while the UE is moving. Therefore, in what follows, we propose a parameterized precoder based on two real-valued scalar parameters to control the width and shape of the beam, respectively. Besides reducing complexity and improving scalability of the optimization, this allows us to precalculate a look-up table for the beam parameters, which can be used during communication. The parameterization is based on the idea, that the tradeoff between increasing communication range on the one hand and improving robustness towards AoD uncertainty on the other hand can be tackled by dynamic beamwidth adaptation.

Figure 3 illustrates the potential benefit from variable-beamwidth precoding in the presence of user mobility. As the UE moves from position $\boldsymbol{p}_{k-1}$ to $\boldsymbol{p}_k$, the BS's estimate of the UE's position at time step k is $\hat{\boldsymbol{p}}_k$. Forming a narrow beam (shown in blue) toward the expected location of the UE would most likely lead to an outage as the transmit and receive beams are misaligned and very low power is received by the UE. However, when forming a wider beam (shown in red), the user would still be covered by the main lobe, making communication more reliable despite AoD uncertainty. In particular, we expect a wider beam to be more robust if the AoD estimation error variance is high, while a narrow beam should be preferred when the AoD estimation is sufficiently accurate. However, since the THz band suffers from particularly severe path loss depending on the distance d_k and the molecular absorption coefficient, ensuring sufficiently high signal strength at the receiver is also a key factor in the beamformer design. Hence, we are facing a tradeoff between increasing the probability of covering the user and enhancing the received signal strength. We tackle this challenge by considering the optimization problem (18) with a parameterized variable beamwidth precoder, which we propose next.

Remark 1. *As previously explained, we propose a parameterization of the precoder for computational complexity and scalability reasons. To demonstrate the accuracy of our parameterization, we also solve* (18) *for a general beamforming vector* $\boldsymbol{f}_k$ *and compare the achievable Pareto region of the general and the parameterized solution in the simulation section. To find a local optimum of the general problem, we apply gradient ascent method. However, since* (18) *is a non-convex problem, numerical optimization does not lead to a unique solution. Therefore, we repeat the gradient ascent for different initial values of* $\boldsymbol{f}_k$ *and pick the best locally optimal solution. Although we cannot claim our general solution to be a global optimum, we gain insights regarding the achievability region and validate the usefulness of our parameterization.*

A. Adaptive Beamwidth Precoder

In this section, we derive a dynamic beamwidth adaptation scheme based on a parameterized precoder. Notice that a wide beam can be formed by adding up multiple beams, which are slightly offset from the expected UE's direction, as it has been done for a multi-resolution codebook design in [38]. In contrast to [38], we sum up infinitely many beams within a certain angular range parameterized by $v \in [0, 1]$, which leads to a precoder of the following form:

$$\boldsymbol{f}(v, \omega) = \frac{\beta}{2v} \int_{-v}^{v} \boldsymbol{u}(\hat{\varphi}, \xi) e^{j\omega\xi} \mathrm{d}\xi, \tag{20}$$

where β is a scaling factor that ensures the transmit power constraint and

$$\boldsymbol{u}(\hat{\varphi}, \xi) = \left[1,\ e^{j\pi(\sin(\hat{\varphi})-\xi)},\ \ldots,\ e^{j\pi(N-1)(\sin(\hat{\varphi})-\xi)}\right]^T. \tag{21}$$

The additional phase shift given by the parameter ω helps optimize the beam shape. Hence, the n-th component of the precoding vector can be determined in closed form, as follows:[5]

$$\begin{aligned} [\boldsymbol{f}(v, \omega)]_n &= \frac{\beta}{2v} \int_{-v}^{v} e^{j\pi n(\sin(\hat{\varphi})-\xi)} e^{j\omega\xi} \mathrm{d}\xi \\ &= \beta \frac{\sin\left((\omega - \pi n)v\right)}{(\omega - \pi n)v} e^{j\pi n \sin(\hat{\varphi})}. \end{aligned} \tag{22}$$

We adopt the precoder (22) when considering the optimization problem (18). In particular, when inserting (22) and (2) in (19),

[5]This beamforming structure is related to the Slepian sequence used for bandpass filter design, where the energy within a certain frequency interval is maximized [38]. Note that our beamformer is designed with continuous phase shifts. While the design of electronically controllable phase shifters with continuous tunability is an active topic of research (e.g. [39]), our beamforming scheme could work with discrete phase shifters with adequate resolution by quantization of the phase. However, a profound analysis of the impact of such hardware restrictions is worthwhile to investigate in future work.

we obtain the following rate expression:

$$R_k = W \log_2 \left(1 + \frac{\beta_k^2 \eta^2(d_k)}{N_\mathrm{t}\sigma_n^2} \times \left| \sum_{n=0}^{N_\mathrm{t}} \frac{\sin\left((\omega_k - \pi n)v_k\right)}{(\omega_k - \pi n)v_k} e^{j\pi n(\sin(\hat{\varphi}_{\mathrm{t},k}) - \sin(\hat{\varphi}_{\mathrm{t},k} + \varepsilon_k))} \right|^2 \right), \tag{23}$$

where $\varepsilon_k = \varphi_{\mathrm{t},k} - \hat{\varphi}_{\mathrm{t},k}$. Hence, the optimization problem (18) reduces to:

$$\begin{aligned} \max_{v_k, \omega_k, \beta_k} \quad & \alpha \, \frac{\mathbb{E}\left[R_k | \boldsymbol{f}_k(v_k, \omega_k), q_k = 0\right]}{R_{\max}} \\ & - (1-\alpha)\Pr(R_k < R_{\min} | \boldsymbol{f}_k(v_k, \omega_k), q_k = 0) \\ \text{s.t.} \quad & \beta_k^2 \sum_{n=0}^{N_\mathrm{t}-1} \frac{\sin^2\left((\omega_k - \pi n)v_k\right)}{(\omega_k - \pi n)^2 v_k^2} \leq P_{\max}. \end{aligned} \tag{24}$$

Next, we derive the approximate expressions for the two objectives, namely the expected rate and the outage probability, before numerically solving (24). First, we assume $d_k \approx \hat{d}_k$ and consider only the distribution of the AoD when applying the expectation operator to the data rate in (23). However, the expectation can still not be easily solved in closed form and is therefore calculated numerically using an integral expression. Note that when maximizing the expected data rate, the optimal beam parameters depend on the SNR as well as the distribution of the AoD $\varphi_{\mathrm{t},k}$. In order to enable a low-complexity look-up table based offline calculation of the optimal beamformer, we combine the AoD estimate $\hat{\varphi}_{\mathrm{t},k}$ and the AoD error variance σ_ε^2 in a single variable by means of the following approximation: Under the assumption that ε_k is small, and utilizing the approximations $\sin(x) \approx x$ and $\cos(x) \approx 1$ for very small x, we have:

$$\begin{aligned} & \sin(\hat{\varphi}) - \sin(\hat{\varphi} + \varepsilon) \\ = & \sin(\hat{\varphi}) - [\sin(\hat{\varphi})\cos(\varepsilon) + \cos(\hat{\varphi})\sin(\varepsilon)] \approx \cos(\hat{\varphi})\varepsilon. \end{aligned} \tag{25}$$

Let $\tilde{\varepsilon}_k = \cos(\hat{\varphi}_{\mathrm{t},k})\varepsilon_k$. Then, $\tilde{\varepsilon}_k \sim \mathcal{N}(0, \tilde{\sigma}^2_{\varepsilon_k})$ with $\tilde{\sigma}^2_{\varepsilon_k} = \cos(\hat{\varphi}_{\mathrm{t},k})^2 \sigma^2_{\varepsilon_k}$ and the PDF of $\tilde{\varepsilon}_k$ is $g_k(\tilde{\varepsilon}_k)$ according to (10). Hence, the expected rate can be written as:

$$\mathbb{E}[R_k] \approx W \int_{-\pi/2}^{\pi/2} \log_2 \left(1 + \frac{\beta_k^2 \eta^2(\hat{d}_k)}{N_\mathrm{t}\sigma_n^2} \times \left| \sum_{n=0}^{N_\mathrm{t}-1} \frac{\sin\left((\omega_k - \pi n)v_k\right)}{(\omega_k - \pi n)v_k} e^{j\pi n \tilde{\varepsilon}_k} \right|^2 \right) g_k(\tilde{\varepsilon}_k) \mathrm{d}\tilde{\varepsilon}_k. \tag{26}$$

Next, we consider the outage probability. Since a closed form expression cannot be easily obtained, we use a logistic function with smoothness parameter θ to approximate the objective instead [40]:

$$P_{\mathrm{out},k} = \Pr(R_k < R_{\min}) \approx \mathbb{E}\left[\frac{1}{1 + \exp(-\theta(R_{\min} - R_k))}\right]. \tag{27}$$

Hence, with (23) and (25), we approximate the outage probability as in (28), shown at the top of the next page.

Using both (26) and (28), we solve Problem (24) using a particle swarm optimization method [41]. The optimal beam parameters v_k and ω_k can be pre-calculated offline for varying $\sigma_{\tilde{\varepsilon}_k}$ and $\hat{d}_k$, generating a look-up table prior to transmission. Due to the beam parameterization, the two optimized scalar beam parameters can be easily stored for different transmission distances and AoD variance to be utilized later for beam adaptation in every time step. Thus, the computational complexity of the numerical optimization is not considered detrimental.

Remark 2. *Since the parameterized precoding structure in* (22) *is based on a sinc-function, $|[\boldsymbol{f}(v,\omega)]_n|$ can be very small for some antennas, due to the zeros of the sinc-function and its decreasing envelope. As a result, some of the antennas will transmit with very low power and, hence, their impact on the beam is insignificant. As a consequence, the energy consumption that is necessary to operate the antenna array can possibly be reduced by applying a simple threshold-based dynamic antenna selection strategy and thereby reducing the number of active antennas. As an example, assume that the beam parameters are $v = 0.1$ and $\omega = 0$ and the ULA consists of $N_\mathrm{t} = 64$ elements. Then, if we decide to turn off all antenna elements that are supposed to transmit less than 5% of the maximum power allocated to a single antenna, only 39 elements would be activated. Thus, in this example, the number of active antennas could be reduced by almost 40% without significantly affecting the communication performance.*

In the following section, we propose a solution to the optimization of q_k in problem (14) and suggest an algorithm for the overall tracking and transmission procedure.

IV. Event-based Tracking Algorithm

A. Event trigger

Recall that q_k is a binary variable that is equal to one when a new channel estimation is performed, and equal to zero otherwise. In other words, we assume to have perfect CSI available at the BS when $q_k = 1$ and outdated CSI with a Gaussian distributed user position error if $q_k = 0$. Thus, while evaluating the objective function for these two cases is manageable, the challenge for solving problem (14) lies in the long-term average overhead constraint (13). To handle this constraint, we use the Lyapunov optimization framework [42], which involves defining a virtual queue that indicates the current deviation from the time-average constraint. Subsequently, this virtual queue is stabilized via Lyapunov optimization, which ensures compliance with the long-term constraint. Hence, for our problem, we define a virtual queue Z with $Z_0 = 0$ as follows:

$$Z_k = \max\{0,\ Z_{k-1} + q_k - r_\mathrm{q}\}. \tag{29}$$

The corresponding Lyapunov function is given as $L(Z_k) = \frac{1}{2}Z_k^2$. Thus, the Lyapunov drift is

$$\begin{aligned} \Delta(Z_k) &= \mathbb{E}\left[L(Z_k) - L(Z_{k-1}) | Z_k\right] \\ &= \mathbb{E}\left[Z_{k-1}(q_k - r_\mathrm{q}) + \frac{1}{2}(q_k - r_\mathrm{q})^2\right]. \end{aligned} \tag{30}$$

Moreover, let $G^{(\mathrm{imp})}_{\alpha,k} = \max_{\boldsymbol{f}_k} g_\alpha(\boldsymbol{f}_k, q_k = 0)$ be the optimal objective function value given that imperfect CSI with distribution determined by $\sigma_{\mathrm{p},k}$ is available at the BS, whereas $G^{(\mathrm{p})}_{\alpha,k} = \max_{\boldsymbol{f}_k} g_\alpha(\boldsymbol{f}_k, q_k = 1)$ denotes the best achievable

$$\Pr(R_k < R_{\min}) \approx \mathbb{E}\left[\left(1 + 2^{-\theta R_{\min}/W}\left(1 + \frac{\eta^2(\hat{d}_k)}{\sigma_{\mathrm{n}}^2}\left|\boldsymbol{a}_{\mathrm{t}}^H(\varphi_{\mathrm{t},k})\boldsymbol{f}(v_k,\omega_k)\right|^2\right)^{\theta}\right)^{-1}\right]$$
$$\approx \int_{-\pi/2}^{\pi/2}\left(1 + 2^{-\theta R_{\min}/W}\left(1 + \frac{\beta_k^2\eta^2(\hat{d}_k)}{N_{\mathrm{t}}\sigma_n^2}\left|\sum_{n=0}^{N_{\mathrm{t}}-1}\frac{\sin\left((\omega_k-\pi n)v_k\right)}{(\omega_k-\pi n)v_k}e^{j\pi n\tilde{\varepsilon}_k}\right|^2\right)^{\theta}\right)^{-1} g_k(\tilde{\varepsilon}_k)\mathrm{d}\tilde{\varepsilon}_k. \tag{28}$$

value of the objective function under the assumption of perfect CSI. Then, the subproblem of optimizing q_k in (14) can be formulated as:

$$\begin{aligned} \max_{q_k} \quad & q_k G_{\alpha,k}^{(\mathrm{p})} + (1-q_k)G_{\alpha,k}^{(\mathrm{imp})} - \mu\Delta(Z_k) \\ \text{s.t.} \quad & \lim_{K\to\infty}\frac{1}{K}\sum_{k=1}^{K} q_k \le r_{\mathrm{q}}. \end{aligned} \tag{31}$$

Here, $\mu > 0$ is a predefined weighting parameter. Note that constraint (12) is independent of q_k and can be neglected in this subproblem. Hence, the solution of (31) is obtained by:

$$q_k = \begin{cases} 1 & \text{if } Z_{k-1} - r_{\mathrm{q}} + \frac{1}{2} < \frac{1}{\mu}(G_{\alpha,k}^{(\mathrm{p})} - G_{\alpha,k}^{(\mathrm{imp})}), \\ 0 & \text{otherwise.} \end{cases} \tag{32}$$

Note that (32) is based on a dynamic condition that adapts to the system state and hence differs from other state-of-the-art approaches that are based on a fixed threshold.

Let $p_{\mathrm{b},k} = P(\gamma_k = 0|\gamma_{k-1})$ be the instantaneous blockage probability estimated by the BS at time step k as given in (7). Then, with (16), we have $\max_{\boldsymbol{f}_k}\ \mathbb{E}[R_k|q_k = 1] = (1-p_{\mathrm{b},k})R_{\max}$. Hence, the objective function value with perfect CSI at the BS is obtained by:

$$G_{\alpha,k}^{(\mathrm{p})} = \begin{cases} \alpha - p_{\mathrm{b},k} & \text{if } W\log_2\left(1 + \frac{P_{\max}\eta^2(\hat{d}_k)}{\sigma_{\mathrm{n}}^2}\right) \\ & \quad \ge R_{\min} \\ (1-p_{\mathrm{b},k})\alpha - (1-\alpha) & \text{otherwise.} \end{cases} \tag{33}$$

The objective function with imperfect CSI $G_{\alpha,k}^{(\mathrm{imp})}$ is computed based on (26) and (28) using the optimal beam parameters corresponding to $\sigma_{\tilde{\varepsilon}_k}$ and d_k. Note that these can be precalculated and saved in a look-up table along with the corresponding objective function values.

B. Tracking Algorithm

Next, we present our framework for the beam tracking and data transmission procedure, including the previously proposed robust beamforming and event-based channel estimation schemes. The dynamic beamwidth adaptation method improves communication reliability despite outdated CSI by tolerating a higher AoD uncertainty than non-robust beamforming, and therefore requires less frequent channel estimation. However, since the variability of the channel caused by user mobility is not uniform in general, we optimized the time steps at which channel estimation should be performed to ensure timely CSI updates without violating the predefined acceptable amount of overhead on average. However, communication outages can still take place for different reasons, namely dynamic blockage, beam misalignment or exceeding the BS's THz communication range. These events require appropriate reactions, like initiating a new channel estimation, adapting the beamformer or conducting a BS handover. Therefore, in the following, our proposed two-fold scheme is embedded into a communication and tracking procedure.

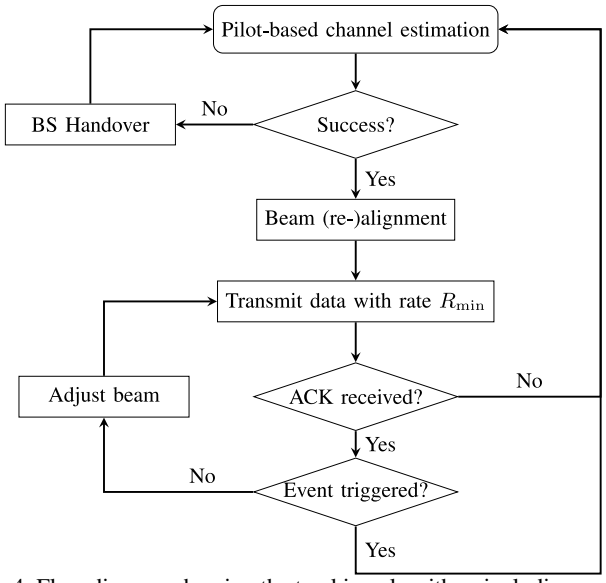

Fig. 4: Flow diagram showing the tracking algorithm, including event-based pilot transmission and handovers.

The overall tracking algorithm is shown in Figure 4. When the considered UE is assigned to a BS, the BS obtains the current CSI through pilot measurements. After successful channel estimation, beam alignment is performed and data is transmitted with rate $R_{\min}$. At the end of a time slot, the BS receives a feedback in the form of an ACK signal if decoding was successful at the UE, while the lack of an ACK signal is interpreted as a decoding failure (NACK). We assume that decoding fails only if the actual data rate R_k supported by the channel is below the transmit data rate $R_{\min}$. Note that this can occur due to either beam misalignment or blockage, or both. If an outage occurs, i.e., the BS did not receive an ACK signal, another pilot signal transmission is invoked to realign the beam. If the current transmission path is blocked and another sufficiently strong propagation path can be detected, the beam is adjusted to switch to the strongest available path. We assume that in case of a total channel blockage event (i.e., if no sufficiently strong reflection path is available), the channel estimation will fail. In this case, a handover is initiated to assign the UE to a different BS with better channel conditions. We then switch our perspective to the new serving

BS and from then on consider the transmission of the new tagged BS-UE pair. Otherwise, when the transmitted signal can be successfully decoded by the UE, i.e., the BS received an ACK signal, the event-triggering condition (32) is checked after each time slot. As long as no pilot transmission event is triggered, the BS will adapt the beamformer and continue to transmit data in the next time slot.

Remark 3. *Note that we strive to account for all phenomena that are relevant to the practicality of our research, while making reasonable assumptions to maintain clarity and tractability of our work. To make our scheme compatible with low-latency demands of 6G applications, our beamforming solution is designed to support cloud-based offline pre-calculation and storage of the optimal beam parameters at the BS for quick access during transmission. Moreover, the beam realignment intervals are typically at a much larger time scale than the transmission time slots in 6G low-latency communication [43]. In fact, since our event-driven approach requires less frequent beam adjustments, it reduces the channel estimation overhead and thereby minimizes the overall delay. To handle communication outages, our proposed tracking scheme comprises CSI estimation and beam realignment as well as BS handovers, yet we do not cover retransmissions as those would most likely entail further outages in the following time steps in our considered scenario. This is because channel blockage or beam misalignment persist for a longer period of time if no other actions are taken such as an updated channel measurement or handover. Note that some aspects that are out of the scope of this paper but worthwhile to investigate in future work include experimental validation of our scheme as well as the consideration of uplink transmission and the impact of hardware restrictions such as discrete phase shifters.*

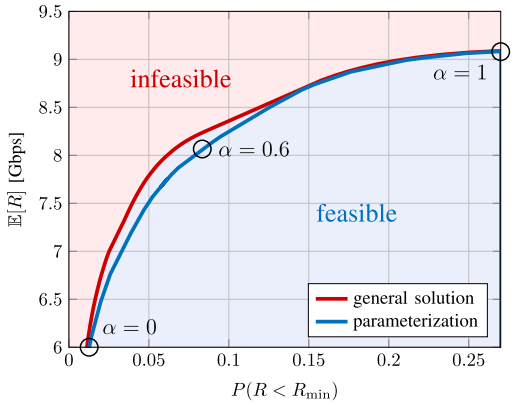

(a) Pareto region

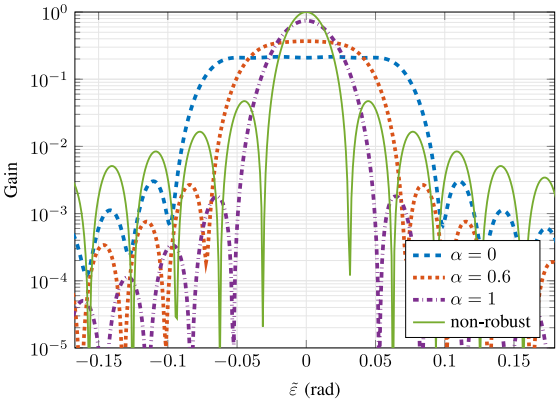

(b) Beam pattern

Fig. 5: (a) Pareto boundary and feasible region of the generally optimized beamformer and the achievable region of the proposed parameterized beamformer, with $R_{\min} = 5$ Gbps, $d = 8$ m, and $\sigma_{\tilde{\varepsilon}} = 1.5°$. (b) Beam pattern with optimized parameters corresponding to the three points marked in (a) in comparison to the non-robust beam.

V. Simulation Results and Analysis

For performance analysis of our scheme, the simulation parameters in Table I are used unless stated otherwise. First, we analyze our adaptive beamwidth precoding scheme based on Monte-Carlo simulations with given AoD uncertainty. After that, the beamforming is embedded into a beam tracking scenario including RW user mobility for performance evaluation of our proposed event-based tracking approach. While our communication scheme is designed to utilize the strongest available path for transmission in a multipath propagation channel, experimental and ray-tracing studies have shown that the NLOS paths in the THz band are generally very weak compared to the LOS path (by more than 20 dB in THz indoor scenarios [44], [45]). This severe attenuation considerably diminishes the data rate when relying on NLOS transmission. Thus, in our simulations we assume that the target rate can only be achieved through LOS transmission.

A. Beamforming Scheme

We first examine the performance of our variable-beamwidth precoding scheme proposed in Section III. We identify the Pareto boundary by numerically solving the optimization problem (18) with a general precoder as described in Remark 1 for varying weight parameter α. In Figure 5(a), we compare the achievable region of our parameterized beamformer with the general Pareto region for a BS-UE distance of $d = 8$ m and AoD standard deviation $\sigma_{\tilde{\varepsilon}} = 1.5°$. Recall that $\alpha = 0$ corresponds to minimizing the outage probability, whereas $\alpha = 1$ is maximizing the expected rate. In fact, the expected rate and the outage probability are opposing objectives, i.e., increasing the rate expectation comes at the cost of a higher outage probability, while minimizing outages reduces the expected rate. Each of the two objectives alone lead to substantially different beamforming strategies. When minimizing the outage probability ($\alpha = 0$), the expected rate reduces by one third. Maximizing the expected rate ($\alpha = 1$) leads to an increase of the outage probability by a factor of more than 20. Note that when α is close to one, we have to accept a much higher outage probability for a relatively small rate gain. The opposite effect is observed when α is close to zero. This motivates considering a multi-objective optimization problem in order to balance the two objectives. Although our proposed parameterized approach does not fully achieve the Pareto region of a general beamformer, it is shown to clearly be a useful approximation despite its reduced complexity. Especially for higher values of α , the gap between the parameterized and the general solution is negligible. The

TABLE I: Parameters used for the simulations, if not stated otherwise.

Number of ULA antenna elements N_{t} (N_{r})	64 (16)	Bandwidth W	10 GHz
Operating Frequency f	300 GHz	Density of dynamic blockers λ_{B}	0.3 m^{-1}
Molecular Absorption Coefficient $K(f)$	0.0012 m^{-1}	Velocity of dynamic blockers v_{B}	1 m/s
Transmit power $P_{\max}$	30 dBm	Height of BS h_{BS}	3.5 m
Noise power spectral density	-174 dBm/Hz	Height of UE h_{UE}	1.5 m
Time slot duration T_{s}	50 ms	Height of blockers h_{B}	1.8 m
RW step size standard deviation σ_{m}	0.05 m	Unblocking rate μ_{B}	3 s^{-1}

biggest performance gap is observed in the area around $\alpha = 0.5$ when both objectives are balanced. In particular, the parameterization results in an average rate loss of about 0.27 Gbps at most, which corresponds to a rate reduction of approximately 3.4%, whereas the outage probability increases by up to 0.018, i.e., by around 25% at most. Hence, the performance loss of the parameterized beamformer mostly stems from the outage probability minimization.

In Figure 5(b), the beam pattern of the optimized parameterized beams is shown for three cases, namely $\alpha \in \{0, 0.6, 1\}$ in comparison to the non-robust beam. As we can see, the beam gets wider as we take greater account of the outage probability, i.e., as α decreases. However, even for $\alpha = 1$ the chosen beam is wider than the non-robust beam. Besides that, we notice that the beam also gets flatter when α decreases. The reason for that effect lies in the threshold-based definition of outage probability, meaning that outages are reduced when the beam gain is above a threshold for most channel realizations, while the actual value of the gain is less relevant.

Figure 6 shows the optimal beamwidth parameter v that solves (24) for different BS-UE distances d and angular deviation $\sigma_{\tilde{\varepsilon}}$, for the two marginal cases $\alpha = 1$ (Fig. 6(a)) and $\alpha = 0$ (Fig. 6(b)). Since v is directly related to the beamwidth, we gain insights on the optimal beamwidth selection in different scenarios. While $v = 0$ corresponds to the non-robust beamformer, i.e., a narrow beam, a larger value of v widens the beam. Hence, from Figure 6(a), we observe that when maximizing the expected rate, the most prominent factor leading to a wider beam is a higher $\sigma_{\tilde{\varepsilon}}$. Indeed, higher fluctuation of the UE's position necessitates a wider beam to cover any changes of the AoD. Additionally, the figure also shows that at small distances, relying on beamforming to concentrate the power and compensate for the THz propagation loss is not as necessary as for longer distances, i.e., a wide beam is more beneficial to increase robustness when the user is sufficiently close to the BS. For instance, with an AoD standard deviation of $\sigma_{\tilde{\varepsilon}} = 8^\circ$ the optimal beamwidth parameter is 0.1 if the UE is at 8 m distance, but increases to 0.2 if the distance is only 2 m. Clearly, beamforming is inevitable when the power needs to be sustained for a longer range at THz frequency bands. Intuitively, this represents the tradeoff between increasing the probability of coverage with a wider beam when the user's position is uncertain and increasing directivity to enhance the received signal strength when facing severe path loss in the THz band.

In Figure 6(b), when minimizing the outage probability, we again observe an increase in beamwidth for higher AoD uncertainty and a decreasing beamwidth for higher communication distance. However, it is clear that both objectives require significantly different beamforming strategies. In fact, for the most part, outage probability minimization leads to substantially wider beams than expected rate maximization, especially for lower communication distances (below 5m). When the channel gain is sufficiently high, the transmission power can be spread more widely without causing an outage and hence, the outage probability is reduced. However, a higher gain in the directions that are most likely is beneficial when considering the expected rate, hence, a moderate beamwidth is preferred in this case. Additionally, Figure 6(b) shows that for higher AoD uncertainty, the beamwidth depends almost exclusively on the communication distance, i.e., the contour lines become nearly vertical. For instance, at a distance of 4 m the optimal value for v first increases

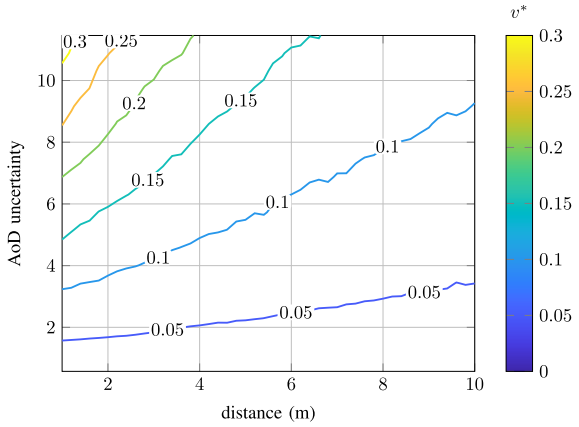

(a) Expected rate maximization ($\alpha = 1$)

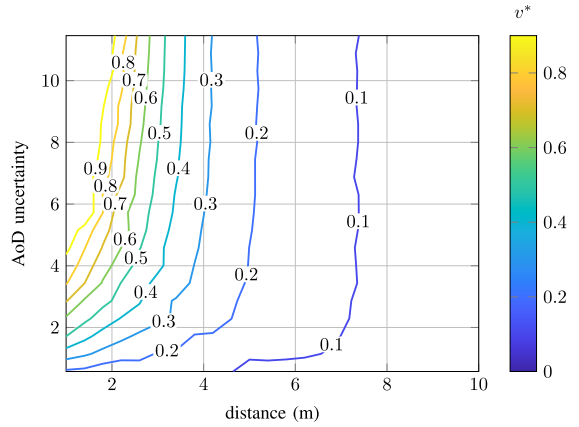

(b) Outage Probability minimzation ($\alpha = 0$)

Fig. 6: Contour plot of the optimized beamwidth parameter v as a function of distance and AoD deviation $\sigma_{\tilde{\varepsilon}}$, for $\alpha = 1$ and $\alpha = 0$. Larger values of v lead to a wider beam, while $v = 0$ corresponds to the non-robust beamformer.

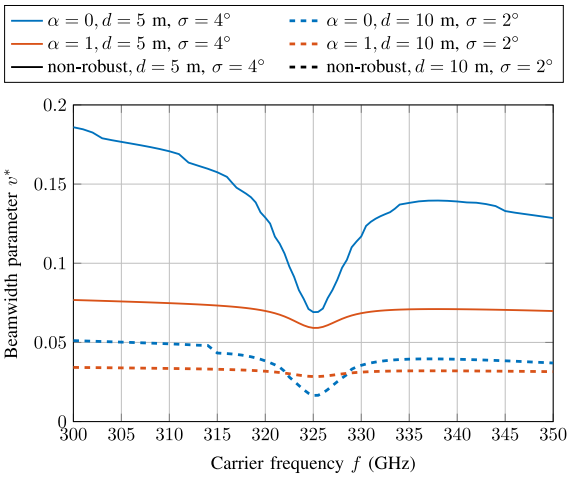

(a) Optimized beamwidth

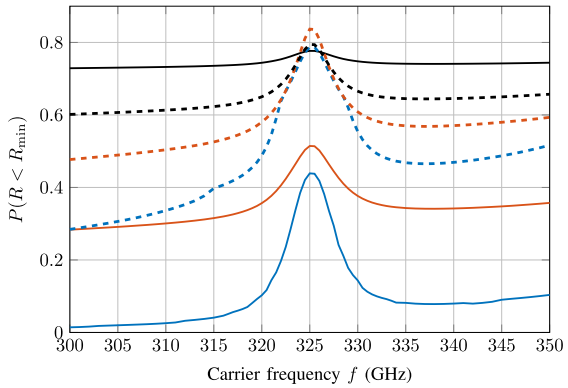

(b) Outage probability

Fig. 7: Impact of molecular absorption on the optimal beamwidth parameter and outage probability with $R_{\min} = 5$ Gbps, shown for outage probability minimization (blue curves) and expected rate maximization (red curves). For both transmission distances of 5 m (solid lines) and 10 m (dashed lines), the misalignment standard deviation is 35 cm, which is equivalent to $4°$ and $2°$ in terms of AoD deviation, respectively.

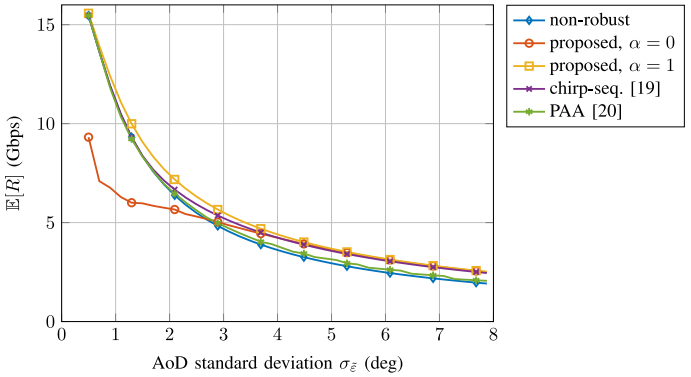

(a) Expected rate

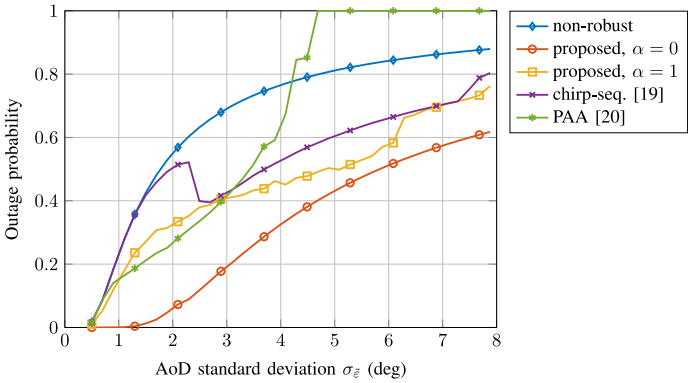

(b) Outage probability

Fig. 8: Expected rate and outage probability as a function of the AoD standard deviation for a communication distance of $d = 8$ m and target rate $R_{\min} = 5$ Gbps. The curves show our proposed beamforming scheme for the marginal cases $\alpha = 0$ and $\alpha = 1$, compared to non-robust beamforming and two baseline schemes.

with growing AoD uncertainty, but remains at a value close to 0.3 for $\sigma_{\tilde{\varepsilon}} > 6°$. Intuitively, this follows from the fact that as soon as the AoD uncertainty becomes detrimental to the outage probability, making the beam as wide as possible is beneficial. Here, despite an increase in the AoD uncertainty, the beamwidth cannot be further increased. Meanwhile, when the communication distance is higher, narrowing the beams is necessary to prevent outages due to the high path loss in the THz band.

Figure 7 showcases the effect of molecular absorption on our proposed beamforming scheme. The optimal beamwidth for maximizing expected rate and minimizing outage probability is shown for the frequency range $[300\text{ GHz}, 350\text{ GHz}]$ in Fig. 7(a). Note that there is an absorption line at around 325 GHz caused by the absorption of the water molecules [22]. Hence, as this frequency band suffers from severe molecular absorption a much narrower beam is required to compensate for this THz-specific factor, which in turn aggravates the susceptibility to beam misalignment. In addition, the beamforming strategy differs substantially for the two objectives. While the absorption line clearly causes a more focused beam in both cases, this impact is much more pronounced when the outage probability is considered as our objective. Since all channel realizations are affected equally by molecular absorption, a small beam adjustment is sufficient when considering expected rate, whereas the beamwidth parameter is more than halved when optimizing the outage probability in order to meet the rate requirement within the main lobe. With good channel conditions, the outage probability objective benefits from a wider beam to prevent misalignment. However, when the channel is heavily affected by molecular absorption, the signal attenuation outweighs the risk of beam misalignment (e.g., with $d = 10$ m, $f = 325$ GHz). Here, narrowing the beam (even more than in the expected rate-focused scheme) becomes a preferred strategy with respect to outage probability. Figure 7(b) shows the probability of the data rate dropping below the target rate of 5 Gbps. Since the outage probability is clearly affected by molecular absorption, optimizing the beamwidth is essential, especially for smaller communication distances, which are common in THz systems, and where the same movement leads to higher AoD deviation. Note that maximizing the expected rate can still lead to many outages caused by misalignment. Furthermore, at a transmission distance of 10 m, we observe that even relatively small changes of the beamwidth can significantly impact the outage probability.

Figure 8 compares our proposed parameterized beamformer to non-robust beamforming and the following two variable-

beamwidth benchmark schemes proposed for mmWave systems:

a) Chirp-sequence-based Beamformer [19]: The authors in [19] proposed a beamforming scheme based on Zadoff-Chu-sequences, where a parameter for beamwidth adjustment is numerically calculated so that the expected data rate is maximized. While the authors suggest to additionally apply a triangular window to the precoder to modify the beam shape, they do not propose a strategy on how to optimally select the window. Therefore, we omit the use of windowing when comparing this scheme to our proposed approach.

b) Partial Antenna Array Activation [20]: The authors in [20] suggest to only activate part of the antenna array in order to form a wider beam. The number of active antennas is determined based on a heuristic, so that the half-power beamwidth approximately covers the range $[\hat{\varphi} - \sigma_{\tilde{\varepsilon}}, \hat{\varphi} + \sigma_{\tilde{\varepsilon}}]$. Note that different from our scheme and the one in [19], the beamwidth is completely independent of the SNR and path loss.

We analyze the expected rate and the outage probability as a function of the AoD standard deviation for a fixed communication distance $d = 8$ m in the Figures 8(a) and 8(b), respectively. While the expected rate decreases with growing AoD uncertainty for all schemes, Figure 8(a) demonstrates the superiority of our proposed approach with $\alpha = 1$ in terms of the expected rate for all $\sigma_{\tilde{\varepsilon}}$. Note that our scheme with $\alpha = 0$, where outage probability is the only objective considered, achieves a much lower average rate than all baselines for $\sigma_{\tilde{\varepsilon}} < 2.5°$, but converges to the expected rate achieved by the scheme with $\alpha = 1$ as $\sigma_{\tilde{\varepsilon}}$ increases. The chirp-sequence based approach from [19], which also aims at maximizing the expected rate, performes similar to the non-robust beamformer when $\sigma_{\tilde{\varepsilon}}$ is low, and only converges to the rate achieved by our proposed scheme for higher AoD uncertainty ($\sigma_{\tilde{\varepsilon}} > 4°$). The partial antenna activation scheme [20] is based on a heuristic and neither maximizing expected rate nor minimizing outage probability explicitly. In terms of rate expectation, it is shown to be just slightly better than the non-robust beamforming, with a gap of around 0.6 Gbps to our proposed scheme. Figure 8(b) compares the outage probability of the respective beamforming approaches. Here, our proposed scheme with $\alpha = 0$, in which the outage probability is minimized, proves to be superior to all baselines for all $\sigma_{\tilde{\varepsilon}}$. Most significantly, for $\sigma_{\tilde{\varepsilon}} < 1.5°$, it has a considerably smaller slope than all other schemes, and up to $\sigma_{\tilde{\varepsilon}} = 3°$, the gap in outage probability is around 0.2. Note that none of the benchmark schemes are designed to minimize outage probability.

B. Beam Tracking Simulation

Next, we simulate the beam tracking scenario with RW mobility of the UE and parameters in Table I. For these simulations, a look-up table with the optimal beam parameters is generated on the grid $d \in [1, 10]$ m (increments 0.2 m) and $\sigma_{\tilde{\varepsilon}} \in [0.01, 0.3]$ (increments 0.01). Note that the time slot duration is set to 50 ms, as the UE is still likely to remain within the main lobe during that time frame for the scale of mobility considered in our simulations. As previously

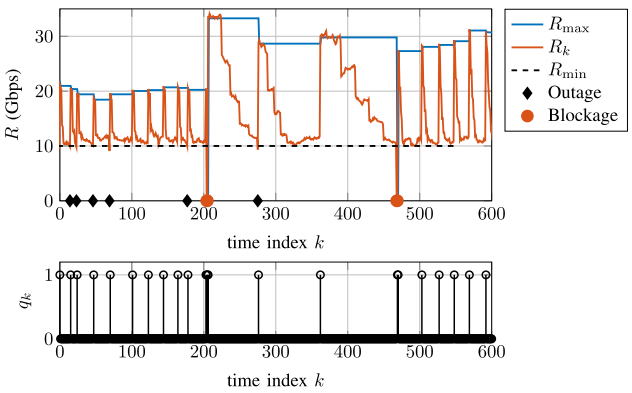

(a) Time sequence example

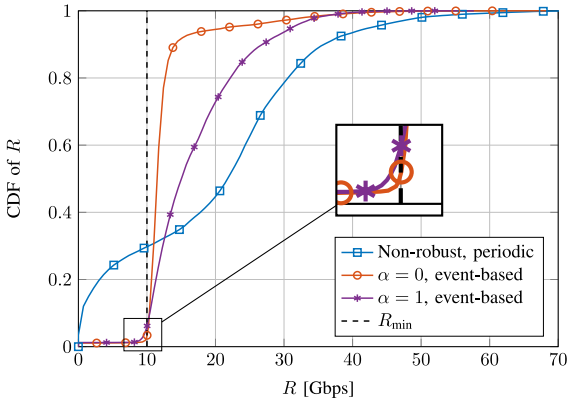

(b) CDF of achievable rate

Fig. 9: Illustration of the event-based tracking procedure with $r_{\mathrm{q}} = 0.05$ and target rate $R_{\min} = 10$ Gbps: (a) Example of achievable data rate over time with corresponding pilot transmission event times, (b) CDF of the data rates achieved by our proposed scheme compared to a non-robust baseline with periodic pilot transmission.

explained, we assume that the target rate cannot be achieved through reflection paths and thus only consider the LOS path in our simulation. In Figure 9, we analyze the achievable rates when using our proposed beamforming scheme combined with the event-based tracking scheme according to (32) with $\mu = 0.5$ and average overhead limitation $r_{\mathrm{q}} = 0.05$, while the target rate is set to $R_{\min} = 10$ Gbps. Figure 9(a) illustrates the event-driven behaviour for a period of 600 time steps. The upper graph shows the rate with perfect CSI as expected by the BS, namely $R_{\max}$, as well as the actual achievable rate with the selected beamformer (as in Section III-A with $\alpha = 0.6$), denoted by R_k. Note that $R_{\max}$ stays constant in between CSI estimation events. The bottom graph shows the corresponding event times given by q_k. While a nearly periodic pilot pattern can be observed for certain time spans (e.g. $k \in [500, 600]$), the channel estimation events occur in a non-uniform manner in general. In particular, when an outage occurs (represented by a black diamond shape), i.e., R_k drops below the target rate $R_{\min}$, a new channel estimation is initiated. A handover is performed to handle blockages (depicted as a red circle). In the evaluation, we pick a serving BS at a random position in the range of 3 to 7 meters apart from the user to simulate a handover. Note that these immediate reactions to outage and blockage events lead to an increase in overhead, which can be observed, e.g., $k \in [0, 70]$, as well as around $k = 170$ and

$k = 205$. In the subsequent time steps, the interval between pilot transmission events is increased to compensate for the excess overhead. Furthermore, the user's relative position to the BS has an impact on the frequency of pilot events as well. This phenomenon can be observed at $k = 205$, where a blockage event induces a handover to a BS that is better placed and allows for much longer intervals between pilots. This event-based scheme makes the data transmission more efficient, since the system can prevent outages resulting from beam misalignment by performing regular channel estimations, while still being able to immediately react to outage and blockage events without violating the average overhead constraint in the long term.

Next, 9(b) shows the cumulative distribution function (CDF) of the data rates achieved by the proposed beamforming and tracking scheme for $\alpha = 0$ and $\alpha = 1$, compared with a non-robust beamformer with periodic pilot measurements. The CDF of our proposed event-based approach with $\alpha = 1$ is below the non-robust CDF for low data rates (below 13 Gbps). This is because our variable beamwidth precoder exhibits a smaller prospect for a low data rate, which is reduced even further by the event-based tracking approach. Meanwhile, the CDF of our event-based scheme grows above the non-robust CDF beyond 13 Gbps since very high data rates (higher than 30 Gbps) are also less likely. For our proposed scheme with $\alpha = 0$, which minimizes the outage probability, the CDF is the lowest for data rates below the target rate $R_{\min}$, but then rapidly grows above the other CDFs. When this scheme is applied, most data rates lie between 10 and 15 Gbps. Although the non-robust baseline enables more high data rates (above 30 Gbps) than our proposed schemes, there are also much more low rates in this case. More precisely, around 30% of the rates are below the target rate of 10 Gbps with the non-robust scheme, while this is the case for only 3% ($\alpha = 0$) and 6% ($\alpha = 1$) of the rates achieved with the other two schemes.

Since we are interested in reliable communication, we study the relation between the frequency of outage events and pilot transmission overhead in Figure 10 and study the efficiency of our event-based channel estimation scheme compared to periodic pilot transmission. Indeed, while our proposed beamformer as well as the event-based tracking approach used individually can significantly reduce the amount of outages compared to non-robust periodic tracking, a combination of both proposed schemes enables much more reliable and efficient communication. With periodic channel estimation, our proposed beamforming scheme with $\alpha = 0.6$ reduces the amount of outages by more than 50% compared to non-robust beamforming. When applying the proposed event-triggered scheme, the actual average overhead can differ from the selected r_{q}. In fact, with the event-based, but non-robust scheme the average overhead is at least 0.083, i.e., there is no feasible solution when r_{q} is below this value. This is because the tracking procedure in Figure 4 enforces pilot signal transmission following each outage event regardless of the overhead constraint. With the combination of the proposed precoding and event-based tracking scheme, however, the average overhead is far below r_{q}. Moreover, the outage probability is substantially lower than in all other cases, namely below 3% for all r_{q}. Indeed, an outage probability slightly below 3% is achieved by the proposed combined scheme with one pilot event every 23 time steps on average, while the proposed BF with periodic channel estimation requires one pilot event every 5 time steps to achieve the same. Hence, we prove that the combination of our proposed beamwidth adaptation approach and an event-triggered tracking scheme significantly improves communication reliability, while requiring substantially less overhead on average.

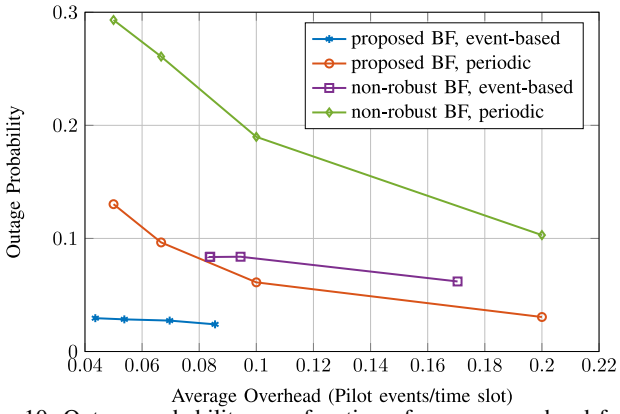

Fig. 10: Outage probability as a function of average overhead for a beam tracking simulation over 100000 time steps, with target rate $R_{\min} = 10$ Gbps, $\alpha = 0.6$ and an overhead constraint with $r_{\mathrm{q}} \in \{0.05,\ 0.667,\ 0.1,\ 0.2\}$.

VI. Conclusion

In this paper, we have proposed a reliable low-overhead communication scheme for a beam tracking scenario in the THz frequency band. Given the adoption of narrow pencil beams at THz communication links, beam misalignment is a fundamental challenge for mobile users that needs to be addressed. Consequently, in this work, we scrutinize the trade-off between increasing coverage probability and supporting a considerable communication range at THz frequencies. In particular, we have formulated a multi-objective optimization problem that maximizes the expected data rate and minimizes the outage probability. We have proposed a dynamic beamwidth adaptation scheme based on a parameterized precoder. In order to maintain a low channel estimation overhead, an event-based tracking scheme has been presented, which dynamically adjusts the pilot transmission intervals in the presence of user mobility and dynamic blockage. Simulation results show that our proposed precoder outperforms state of the art adjustable beamwidth approaches. Our scheme has been shown to significantly reduce the amount of communication outages without violating restrictions on the average overhead.

References

[1] C. Chaccour and W. Saad, "On the ruin of age of information in augmented reality over wireless terahertz (THz) networks," in *Proc. IEEE Global Commun. Conf. (GLOBECOM)*, Taipei, Taiwan, Dec. 2020, pp. 1–6.

[2] L. U. Khan, W. Saad, D. Niyato, Z. Han, and C. S. Hong, "Digital-twin-enabled 6G: Vision, architectural trends, and future directions," *IEEE Commun. Mag.*, vol. 60, no. 1, pp. 74–80, Jan. 2022.

[3] C. Chaccour, M. N. Soorki, W. Saad, M. Bennis, P. Popovski, and M. Debbah, "Seven defining features of terahertz (THz) wireless systems: A fellowship of communication and sensing," *IEEE Commun. Surveys Tuts.*, vol. 24, no. 2, pp. 967–993, Jan. 2022.

[4] I. F. Akyildiz, C. Han, and S. Nie, "Combating the distance problem in the millimeter wave and terahertz frequency bands," *IEEE Commun. Mag.*, vol. 56, no. 6, pp. 102–108, June 2018.

[5] H. Sarieddeen, M.-S. Alouini, and T. Y. Al-Naffouri, "An overview of signal processing techniques for terahertz communications," *Proc. IEEE*, Oct. 2021.

[6] V. Petrov, D. Moltchanov, Y. Koucheryavy, and J. M. Jornet, "Capacity and outage of terahertz communications with user micro-mobility and beam misalignment," *IEEE Trans. Veh. Technol.*, vol. 69, no. 6, pp. 6822–6827, June 2020.

[7] J. Kokkoniemi, A.-A. A. Boulogeorgos, M. Aminu, J. Lehtomäki, A. Alexiou, and M. Juntti, "Impact of beam misalignment on THz wireless systems," *Nano Commun. Netw.*, vol. 24, p. 100302, May 2020.

[8] W. Chen, L. Li, Z. Chen, H. H. Yang, and T. Q. Quek, "Mobility and Blockage-induced Beam Misalignment and Throughput Analysis for THz Networks," in *Proc. IEEE Global Commun. Conf. (GLOBECOM)*, Madrid, Spain, Dec. 2021, pp. 1–6.

[9] W. Attaoui, K. Bouraqia, and E. Sabir, "Initial Access & Beam Alignment for mmWave and Terahertz Communications," *IEEE Access*, vol. 10, pp. 35 363–35 397, Mar. 2022.

[10] Q. Xia and J. M. Jornet, "Expedited Neighbor Discovery in Directional Terahertz Communication Networks Enhanced by Antenna Side-Lobe Information," *IEEE Trans. Veh. Technol.*, vol. 68, no. 8, pp. 7804–7814, 2019.

[11] Y. Ghasempour, C.-Y. Yeh, R. Shrestha, D. Mittleman, and E. Knightly, "Single Shot Single Antenna Path Discovery in THz Networks," in *Proc. 26th Annu. Int. Conf. Mobile Comput. Netw.*, ser. MobiCom '20. New York, NY, USA: Association for Computing Machinery, 2020.

[12] G. Stratidakis, G. D. Ntouni, A.-A. A. Boulogeorgos, D. Kritharidis, and A. Alexiou, "A low-overhead hierarchical beam-tracking algorithm for THz wireless systems," in *Proc. Eur. Conf. Netw. Commun. (EuCNC)*, Dubrovnik, Croatia, June 2020, pp. 74–78.

[13] J. Park, S. Kim, J. Moon, and B. Shim, "Fast Terahertz Beam Training Via Frequency-dependent Precoding," in *Proc. IEEE Int. Conf. Commun. Workshops (ICC Workshops)*, Seoul, South Korea, May 2022, pp. 1153–1158.

[14] D. Moltchanov, Y. Gaidamaka, D. Ostrikova, V. Beschastnyi, Y. Koucheryavy, and K. Samouylov, "Ergodic outage and capacity of terahertz systems under micromobility and blockage impairments," *IEEE Trans. Wireless Commun.*, vol. 21, no. 5, pp. 3024–3039, Oct. 2021.

[15] B. Ning, Z. Chen, Z. Tian, C. Han, and S. Li, "A Unified 3D Beam Training and Tracking Procedure for Terahertz Communication," *IEEE Trans. Wireless Commun.*, Sept. 2021.

[16] L. Yang and W. Zhang, "Beam tracking and optimization for UAV communications," *IEEE Trans. Wireless Commun.*, vol. 18, no. 11, pp. 5367–5379, Nov. 2019.

[17] C. Liu, M. Li, L. Zhao, P. Whiting, S. V. Hanly, I. B. Collings, and M. Zhao, "Robust adaptive beam tracking for mobile millimetre wave communications," *IEEE Trans. Wireless Commun.*, vol. 20, no. 3, pp. 1918–1934, Nov. 2020.

[18] K. C. Joshi, S. Niknam, R. V. Prasad, and B. Natarajan, "Analyzing the tradeoffs in using millimeter wave directional links for high data-rate tactile internet applications," *IEEE Trans. Ind. Informat.*, vol. 16, no. 3, pp. 1924–1932, July 2019.

[19] R. Peng and Y. Tian, "Robust wide-beam analog beamforming with inaccurate channel angular information," *IEEE Commun. Lett.*, vol. 22, no. 3, pp. 638–641, Mar. 2018.

[20] H. Chung, J. Kang, H. Kim, Y. M. Park, and S. Kim, "Adaptive beamwidth control for mmWave beam tracking," *IEEE Commun. Lett.*, vol. 25, no. 1, pp. 137–141, Jan. 2021.

[21] C. Chaccour, M. N. Soorki, W. Saad, M. Bennis, and P. Popovski, "Can terahertz provide high-rate reliable low latency communications for wireless VR?" *IEEE Internet Things J.*, Jan. 2022.

[22] J. Kokkoniemi, J. Lehtomäki, and M. Juntti, "A line-of-sight channel model for the 100–450 gigahertz frequency band," *EURASIP J. Wireless Commun. Netw.*, vol. 2021, no. 1, pp. 1–15, Apr. 2021.

[23] ——, "A discussion on molecular absorption noise in the terahertz band," *Nano commun. netw.*, vol. 8, pp. 35–45, June 2016.

[24] L. Dai, J. Tan, Z. Chen, and H. V. Poor, "Delay-Phase Precoding for Wideband THz Massive MIMO," *IEEE Trans. Wireless Commun.*, vol. 21, no. 9, pp. 7271–7286, 2022.

[25] L. Miretti, T. Kühne, A. Schultze, W. Keusgen, G. Caire, M. Peter, S. Stańczak, and T. Eichler, "Little or no equalization is needed in energy-efficient sub-THz mobile access," *arXiv preprint arXiv:2210.05806*, 2022.

[26] D. Liu, Y. Wang, P. He, Y. Zhai, and H. Wang, "TOA localization for multipath and NLOS environment with virtual stations," *EURASIP J. Wireless Commun. Netw.*, vol. 2017, no. 1, pp. 1–7, 2017.

[27] I. K. Jain, R. Kumar, and S. S. Panwar, "The impact of mobile blockers on millimeter wave cellular systems," *IEEE J. Sel. Areas Commun.*, vol. 37, no. 4, pp. 854–868, Apr. 2019.

[28] M. Gapeyenko, A. Samuylov, M. Gerasimenko, D. Moltchanov, S. Singh, M. R. Akdeniz, E. Aryafar, N. Himayat, S. Andreev, and Y. Koucheryavy, "On the Temporal Effects of Mobile Blockers in Urban Millimeter-Wave Cellular Scenarios," *IEEE Trans. Veh. Technol.*, vol. 66, no. 11, pp. 10 124–10 138, 2017.

[29] C. Chaccour, M. N. Soorki, W. Saad, M. Bennis, and P. Popovski, "Risk-based optimization of virtual reality over terahertz reconfigurable intelligent surfaces," in *Proc. IEEE Int. Conf. Commun. (ICC)*, Dublin, Ireland, June 2020, pp. 1–6.

[30] R. Di Taranto, S. Muppirisetty, R. Raulefs, D. Slock, T. Svensson, and H. Wymeersch, "Location-aware communications for 5G networks: How location information can improve scalability, latency, and robustness of 5G," *IEEE Signal Process. Mag.*, vol. 31, no. 6, pp. 102–112, 2014.

[31] L. Sanguinetti, A. L. Moustakas, E. Björnson, and M. Debbah, "Large system analysis of the energy consumption distribution in multi-user MIMO systems with mobility," *IEEE Trans. Wireless Commun.*, vol. 14, no. 3, pp. 1730–1745, Nov. 2014.

[32] V. A. Aalo, G. P. Efthymoglou, and C. Chayawan, "On the envelope and phase distributions for correlated Gaussian quadratures," *IEEE Commun. Lett.*, vol. 11, no. 12, pp. 985–987, Dec. 2007.

[33] V. Va, H. Vikalo, and R. W. Heath, "Beam tracking for mobile millimeter wave communication systems," in *Proc. IEEE Global Conf. Signal Inf. Process. (GlobalSIP)*, Washington, DC, USA, Dec. 2016, pp. 743–747.

[34] S. Jayaprakasam, X. Ma, J. W. Choi, and S. Kim, "Robust beam-tracking for mmWave mobile communications," *IEEE Commun. Lett.*, vol. 21, no. 12, pp. 2654–2657, Dec. 2017.

[35] Y. Ge, Z. Zeng, T. Zhang, and Y. Sun, "Unscented Kalman Filter Based Beam Tracking for UAV-enabled Millimeter Wave Massive MIMO Systems," in *Proc. IEEE Int. Symp. Wireless Commun. Syst.*, Oulu, Finland, Aug. 2019, pp. 260–264.

[36] E. Bjornson, E. A. Jorswieck, M. Debbah, and B. Ottersten, "Multiobjective Signal Processing Optimization: The Way to Balance Conflicting Metrics in 5G Systems," *IEEE Signal Process. Mag.*, vol. 31, no. 6, pp. 14–23, Nov. 2014.

[37] D. Xu and Q. Li, "Ergodic Capacity and Outage Probability Optimization for Secondary User in Cognitive Radio Networks under Interference Outage Constraint," *AEU-Int. J. Electron. Commun.*, vol. 68, no. 8, pp. 747–755, Aug. 2014.

[38] S. Noh, M. D. Zoltowski, and D. J. Love, "Multi-resolution codebook and adaptive beamforming sequence design for millimeter wave beam alignment," *IEEE Trans. Wireless Commun.*, vol. 16, no. 9, pp. 5689–5701, Sept. 2017.

[39] P. K. Singh, G. Aizin, N. Thawdar, M. Medley, and J. M. Jornet, "Graphene-based plasmonic phase modulator for Terahertz-band communication," in *10th Eur. Conf. Antennas Propag. (EuCAP)*, 2016, pp. 1–5.

[40] G. Zhou, C. Pan, H. Ren, K. Wang, and M. Di Renzo, "Fairness-Oriented Multiple RISs-Aided MmWave Transmission: Stochastic Optimization Approaches," *arXiv preprint arXiv:2012.06103*, 2020.

[41] D. Wang, D. Tan, and L. Liu, "Particle swarm optimization algorithm: an overview," *Soft Computing*, vol. 22, no. 2, pp. 387–408, Jan. 2017.

[42] M. J. Neely, "Stochastic network optimization with application to communication and queueing systems," *Synthesis Lectures on Communication Networks*, vol. 3, no. 1, pp. 1–211, 2010.

[43] M. Giordani, M. Polese, A. Roy, D. Castor, and M. Zorzi, "A Tutorial on Beam Management for 3GPP NR at mmWave Frequencies," *IEEE Commun. Surveys Tuts.*, vol. 21, no. 1, pp. 173–196, 2019.

[44] J. Kokkoniemi, J. Lehtomäki, and M. Juntti, "LOS and NLOS Channel Models for Indoor 300 GHz Communications," in *16th Int. Symp. Wireless Commun. Syst. (ISWCS)*, 2019, pp. 441–445.

[45] S. Nie and I. F. Akyildiz, "Three-dimensional dynamic channel modeling and tracking for terahertz band indoor communications," in *IEEE 28th Annu. Int. Symp. Pers., Indoor, Mobile Radio Commun. (PIMRC)*, 2017, pp. 1–5.

Yasemin Karaçora (S'17) received her B.Sc. and M.Sc. degree in Electrical Engineering and Information Technology from Ruhr University Bochum, Germany, in 2016 and 2019, respectively. From 2016 to 2017 she was an exchange student at the ECE Department of Purdue University, IN, USA. She is currently pursuing her Ph.D. degree at the Institute of Digital Communication Systems, Ruhr University Bochum, Germany. Her research interests include wireless communication, beamforming at (sub-)terahertz frequency bands, and reliability and resilience in 5G and 6G networks.

Christina Chaccour (S'17-M'23) is currently a Network Solutions Manager at Ericsson, Inc. She received her B.E. in Electrical Engineering from Notre Dame University, Louaize (NDU), Lebanon in 2018. She obtained her M.S. degree and Ph.D. degree in Electrical Engineering from Virginia Tech, VA, USA in 2020 and 2023 respectively. Her research interests include wireless communications, extended reality (XR), 6G systems, terahertz (THz) frequency bands, artificial intelligence, and semantic communications. Her expertise in these areas has led her to derive some of the first performance analysis results on the potential of using 6G systems at THz frequencies to deliver perceptual and haptic requirements for next-generation XR and holographic systems. Dr. Chaccour is the recipient of the Best Paper Award for her peer-reviewed conference paper at the 10th IFIP Conference on New Technologies, Mobility, and Security (NTMS), Canary Islands, Spain, in 2019 and was recognized as an Exemplary Reviewer (fewer than 2%) from IEEE Transactions on Communications in 2021. Additionally, Dr. Chaccour co-founded the startup Internet of Trees (IOTree), which has received numerous local and international awards. She has further gained industry experience through internships at Ericsson Inc., Plano, TX, USA, and Cadence Design Systems, Munich GmBh.

Aydin Sezgin (S'01-M'05–SM'13) received the Dipl.Ing. (M.S.) degree in communications engineering from Technische Fachhochschule Berlin (TFH), Berlin, in 2000, and the Dr. Ing. (Ph.D.) degree in electrical engineering from TU Berlin, in 2005. From 2001 to 2006, he was with the Heinrich-Hertz-Institut, Berlin. From 2006 to 2008, he held a postdoctoral position, and was also a lecturer with the Information Systems Laboratory, Department of Electrical Engineering, Stanford University, Stanford, CA, USA. From 2008 to 2009, he held a postdoctoral position with the Department of Electrical Engineering and Computer Science, University of California, Irvine, CA, USA. From 2009 to 2011, he was the Head of the Emmy-Noether- Research Group on Wireless Networks, Ulm University. In 2011, he joined TU Darmstadt, Germany, as a professor. He is currently a professor of information systems and sciences with the Department of Electrical Engineering and Information Technology, Ruhr-UniversitÃ¤t Bochum, Germany. He is interested in signal processing, communication, and information theory, with a focus on wireless networks. He has published several book chapters more than 65 journals and 200 conference papers in these topics. He has coauthored a book on multi-way communications. Aydin is a winner of the ITG-Sponsorship Award, in 2006. He was the first recipient of the prestigious Emmy-Noether Grant by the German Research Foundation in communication engineering, in 2009. He has coauthored papers that received the Best Poster Award at the IEEE Communication Theory Workshop, in 2011, the Best Paper Award at ICCSPA, in 2015, and the Best Paper Award at ICC, in 2019. He has served as an Associate Editor for the IEEE Transactions on Wireless Communications (2009-2014), and as an area editor for the Elsevier Journal of Electronics and Communications (2010-2011). He was also the General Co-chair of the 2018 International ITG Workshop on Smart Antennas, the program co-chair of the 2019 Crowncom Conference, and the workshop co-chair of the 2022 WCNC workshop on rate-splitting and next generation multiple access.

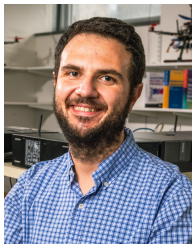

Walid Saad (S'07, M'10, SM'15, F'19) received his Ph.D degree from the University of Oslo, Norway in 2010. He is currently a Professor at the Department of Electrical and Computer Engineering at Virginia Tech, where he leads the Network sciEnce, Wireless, and Security (NEWS) laboratory. He is also the Next-G Wireless Faculty Lead at Virginia Tech's Innovation Campus. His research interests include wireless networks (5G/6G/beyond), machine learning, game theory, security, UAVs, semantic communications, cyber-physical systems, and network science. Dr. Saad is a Fellow of the IEEE. He is also the recipient of the NSF CAREER award in 2013, the AFOSR summer faculty fellowship in 2014, and the Young Investigator Award from the Office of Naval Research (ONR) in 2015. He was the (co-)author of eleven conference best paper awards at IEEE WiOpt in 2009, ICIMP in 2010, IEEE WCNC in 2012, IEEE PIMRC in 2015, IEEE SmartGridComm in 2015, EuCNC in 2017, IEEE GLOBECOM (2018 and 2020), IFIP NTMS in 2019, IEEE ICC (2020 and 2022). He is the recipient of the 2015 and 2022 Fred W. Ellersick Prize from the IEEE Communications Society, and of the IEEE Communications Society Marconi Prize Award in 2023. He was also a co-author of the papers that received the IEEE Communications Society Young Author Best Paper award in 2019, 2021, and 2023. Other recognitions include the 2017 IEEE ComSoc Best Young Professional in Academia award, the 2018 IEEE ComSoc Radio Communications Committee Early Achievement Award, and the 2019 IEEE ComSoc Communication Theory Technical Committee Early Achievement Award. From 2015-2017, Dr. Saad was named the Stephen O. Lane Junior Faculty Fellow at Virginia Tech and, in 2017, he was named College of Engineering Faculty Fellow. He received the Dean's award for Research Excellence from Virginia Tech in 2019. He was also an IEEE Distinguished Lecturer in 2019-2020. He has been annually listed in the Clarivate Web of Science Highly Cited Researcher List since 2019. He currently serves as an Area Editor for the IEEE Transactions on Network Science and Engineering and the IEEE Transactions on Communications. He is the Editor-in-Chief for the IEEE Transactions on Machine Learning in Communications and Networking.